### Title
The structural kinetics of switch-1 and the neck linker explain the functions of kinesin-1 and Eg5




### Journal
Proceedings of the National Academy of Sciences of the United States of America, 112(48)

### ISSN
0027-8424



### Authors
Muretta, Joseph M
Jun, Yonggun
Gross, Steven P
et al.



### Publication Date
2015-12-01

### DOI
10.1073/pnas.1512305112

# The structural kinetics of switch-1 and the neck linker explain the functions of kinesin-1 and Eg5

Joseph M. Muretta[a], Yonggun Jun[b], Steven P. Gross[b,c], Jennifer Major[d], David D. Thomas[a], and Steven S. Rosenfeld[d,1]

[a]Department of Biochemistry, Molecular Biology, and Biophysics, University of Minnesota, Minneapolis, MN 55455; [b]Department of Developmental and Cell Biology, University of California, Irvine, CA 92697; [c]Department of Physics, University of California, Irvine, CA 92697; and [d]Department of Cancer Biology, Lerner Research Institute of the Cleveland Clinic Foundation, Cleveland, OH 44195

Edited by James A. Spudich, Stanford University School of Medicine, Stanford, CA, and approved October 26, 2015 (received for review June 23, 2015)

**Kinesins perform mechanical work to power a variety of cellular functions, from mitosis to organelle transport. Distinct functions shape distinct enzymologies, and this is illustrated by comparing kinesin-1, a highly processive transport motor that can work alone, to Eg5, a minimally processive mitotic motor that works in large ensembles. Although crystallographic models for both motors reveal similar structures for the domains involved in mechanochemical transduction—including switch-1 and the neck linker—how movement of these two domains is coordinated through the ATPase cycle remains unknown. We have addressed this issue by using a novel combination of transient kinetics and time-resolved fluorescence, which we refer to as "structural kinetics," to map the timing of structural changes in the switch-1 loop and neck linker. We find that differences between the structural kinetics of Eg5 and kinesin-1 yield insights into how these two motors adapt their enzymologies for their distinct functions.**

kinesin | transient kinetics | time-resolved fluorescence | molecular motor | fluorescence resonance energy transfer

There are more than 42 kinesin genes in the human genome, representing 14 distinct classes (1). All are members of the P-loop NTPase superfamily of nucleotide triphosphate hydrolases (2–4). Like other NTPases, kinesins share a conserved Walker motif nucleotide-binding fold (2, 4) that consists of a central twisted β-sheet and three nucleotide-binding loops, which are termed switch-1, switch-2, and the P-loop. Kinesins also share a common microtubule (MT) binding interface, which isomerizes between states that either bind MTs weakly or strongly, and a mechanical element, termed the neck linker (NL). The NL has been proposed to isomerize between two conformations: one that is flexible and termed undocked, and the other that is ordered and termed docked, where it interacts with a cleft in the motor domain formed by the twisted β-sheet and is oriented along the MT axis (5–7). NL isomerization (5, 8) is hypothesized to be the force-generating transition in kinesin motors (6, 7, 9–11), and its position has also been proposed to coordinate the ATPase cycles of processive kinesin dimers by regulating nucleotide binding and hydrolysis (11).

Spectroscopic and structural studies have led to a model to explain how kinesins generate force (5–7, 9, 10, 12–15) (summarized in *SI Appendix*, Fig. S1), which proposes that the conformations of the nucleotide binding site, the MT-binding interface, and the NL are all determined by the state of the catalytic site. It predicts that when unbound to the MT, the motor contains ADP in its catalytic site and its NL is undocked. MT binding accelerates ADP dissociation, thereby allowing ATP to bind, the NL to dock, and mechanical work to be performed. ATP hydrolysis and phosphate release are then followed by dissociation from the MT to complete the cycle (5, 7–10, 14). This model also argues that: (*i*) NL docking of the MT-attached motor domain moves the tethered, trailing head into a forward position, where it undergoes a biased diffusional search to attach to the next MT-binding site (11, 14); (*ii*) switch-1, which coordinates the γ-phosphate of ATP, alternates between two conformations, referred to as "open" and "closed," and the NL alternates between docked and undocked (5, 6, 10, 13–15); and (*iii*) coordination between the conformations of switch-1 and the NL regulates the timing of the ATPase cycles of the two motor domains in processive kinesin dimers (11). However, the model fails to explain several features of kinesins. For example, it predicts that ATP does not bind to kinesin when the NL is docked. This prediction is inconsistent with studies of both Eg5 and kinesin-1, which suggest ATP binds more readily when the NL is docked (11, 16, 17). The model also predicts that the NL should be docked after ATP binding. However, electron paramagnetic resonance (EPR) probes attached to the NL show a significant population of both mobile and immobile NL states in the presence of both pre- and posthydrolytic ATP analogs (5). Furthermore, the model cannot explain the load dependence of stall, detachment, and back stepping, all of which require a branched pathway (11).

To resolve these uncertainties, we have measured the kinetics of the structural changes that occur in switch-1 and the NL with nucleotide binding while the motor is bound to the MT in an experimental design that we refer to as "structural kinetics." We carried out these experiments using an novel spectroscopic approach, termed transient time-resolved fluorescence resonance energy transfer, $(TR)^2$FRET, that allows us to monitor the kinetics and thermodynamics of both the undocked/docked transition in the NL and the open/closed transition in switch-1 that accompany the process of nucleotide binding. These experiments explain differences in the enzymologies of kinesin-1 and Eg5 and suggest an interesting role for the L5 loop in controlling the timing of conformational changes in the Eg5 switch-1 and NL.

## Significance

**The kinesins are molecular motors that couple ATP binding to movement. Although crystallographic and cryo-EM methods have identified the structural changes that occur in several kinesins, the images they generate are static pictures that provide no insight into how dynamic these conformations are or how they are coupled together to generate force. We have addressed this through a novel combination of time-resolved fluorescence and transient-state kinetics to measure the conformational equilibria between two key domains in two functionally distinct kinesins: kinesin-1 and Eg5. Our results are significant because they provide a unique insight into how conformational dynamics vary between two kinesins with different functions, and explain the distinct enzymologies these two kinesins have.**

Author contributions: J.M.M., Y.J., S.P.G., D.D.T., and S.S.R. designed research; J.M.M., Y.J., and S.S.R. performed research; J.M.M., J.M., D.D.T., and S.S.R. contributed new reagents/analytic tools; J.M.M., Y.J., S.P.G., D.D.T., and S.S.R. analyzed data; and J.M.M., S.P.G., and S.S.R. wrote the paper.

The authors declare no conflict of interest.

This article is a PNAS Direct Submission.

[1]To whom correspondence should be addressed. Email: rosenfs@ccf.org.

This article contains supporting information online at www.pnas.org/lookup/suppl/doi:10.1073/pnas.1512305112/-/DCSupplemental.

## Results

**Engineering and Characterizing Kinesin-1 and Eg5 Switch-1 and NL FRET Sensors.** We generated cysteine light kinesin-1 and Eg5 constructs with reactive cysteines in the NL and β7 (referred to as $Kin1_{NL}$ and $Eg5_{NL}$) or in switch-1 and β1 (referred to as $Kin1_{Sw1}$ and $Eg5_{Sw1}$). The locations of the reactive cysteine residues (222 and 334 for $Kin1_{NL}$, 21 and 194 for $Kin1_{Sw1}$, 256 and 365 for $Eg5_{NL}$, and 30 and 228 for $Eg5_{Sw1}$) are depicted in Fig. 1*A* for kinesin-1 and Fig. 1*B* for Eg5. These labeling sites were selected based on prior structural studies (2, 6, 7, 9–12, 17–19) to detect changes in the distance between the NL or switch-1 and relatively fixed locations in β1 and β7 by using time-resolved FRET between a fluorescent donor (AEDANS) and a nonfluorescent acceptor (DDPM) (20, 21).

We measured the MT-activated ATPase activities of AEDANS-labeled $Kin1_{NL}$, $Kin1_{Sw1}$, $Eg5_{NL}$, and $Eg5_{Sw1}$ at 20 °C. Comparing these results to those for the unlabeled cysteine light monomeric kinesin-1 and Eg5 constructs (which do not have the additional cysteine insertions in the β-core, NL, or switch-1) (11, 17, 22) reveals that AEDANS labeling reduces $k_{cat}$ by two- to fourfold (*SI Appendix*, Table S1). We measured the kinetics of nucleotide induced MT dissociation of AEDANS-labeled cysteine light kinesin-1, cysteine-light Eg5, $Kin_{Sw1}$, $Kin_{NL}$, $Eg5_{Sw1}$, and $Eg5_{NL}$ constructs by monitoring FRET between the AEDANS fluorophores and MT tryptophans, as described previously (8, 16). *SI Appendix*, Table S2 demonstrates that all of the constructs have rate constants at 20 °C for nucleotide-induced MT dissociation close to wild-type monomeric constructs (8, 16). Our results thus indicate that the reduction in $k_{cat}$ reflects a change in the kinetics of these constructs while detached from the MT, and therefore that the weak-to-strong and strong-to-weak MT binding transitions are not perturbed by labeling.

The cysteine light kinesin-1 construct used by us and by others in prior studies replaces six of the nine cysteines in the motor domain with alanine or serine (5). Although the steady-state and transient kinetic parameters for this mutant kinesin-1 are similar to wild-type, a recent report (23) has noted that these mutations shift the single molecule force velocity relationship toward larger assisting forces. The studies described in the following sections have been performed in the absence of external load, and as we have previously shown, the single molecule unloaded velocity of a dimeric version of this kinesin-1 construct is very similar to wild-type (24). To complete this characterization, we therefore examined the force–velocity relationship of a dimeric cysteine light Eg5 construct that contains the same cysteine mutations in the motor domain as $Eg5_{NL}$; results are summarized in *SI Appendix*, Fig. S2. We fit the data to the same Michaelis–Menten model described in a prior study of a wild-type Eg5 dimer (25), except we used the $K_m$ for ATP measured from the in vitro ATPase activity of our cysteine light version (18 ± 6 μM) (17). This approach provides values of the steady-state ATPase rate, second-order rate constant for ATP binding, and distance to the transition state that are summarized in *SI Appendix*, Table S3, which demonstrates that these parameters are quite similar to the corresponding values for a wild-type Eg5 dimer.

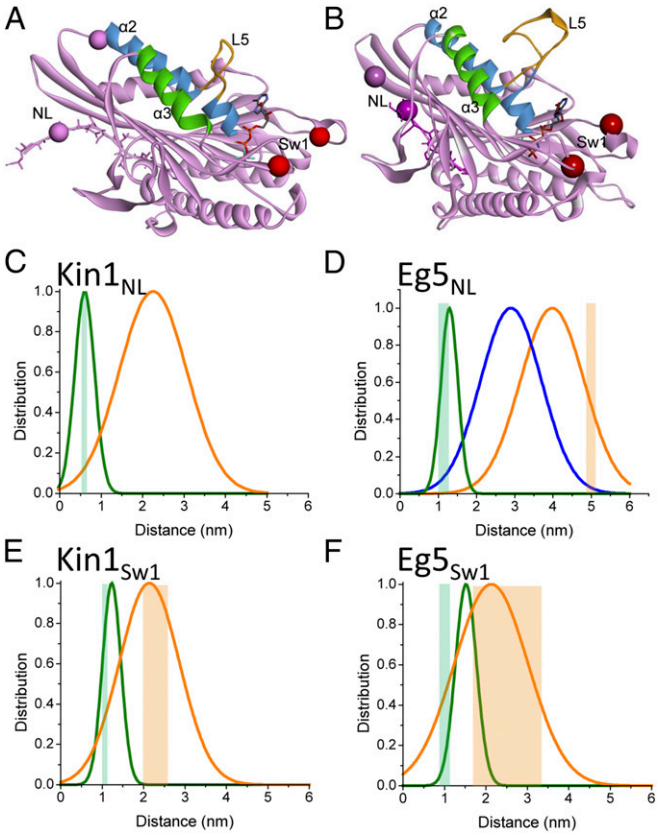


**Fig. 1.** Predicted and measured TR-FRET distance distributions for FRET probes attached to Kin1 and Eg5. (*A* and *B*) Ribbon diagram of Kin1 (*A*, PDB ID code 4HNA) and Eg5 (*B*, PDB ID code 3HQD) showing labeling sites in the NL (magenta spheres) and Sw1 (red spheres). Colored structural elements include α2 (blue), α3 (green), L5 (orange), nucleotide (ball and stick), and docked NL (magenta ball and stick). In both *A* and *B* the NL is docked and switch-1 is closed. (*C*–*F*): Predicted distances (green and orange rectangles, tabulated in *SI Appendix*, Table S5) and measured (solid lines, tabulated in *SI Appendix*, Table S4) distance distributions for NL (*C* and *D*) and Sw1 (*E* and *F*), Kin1 (*C* and *E*) and Eg5 (*D* and *F*) constructs used in this study. Docked and closed distances indicated by green lines, undocked and open distances indicated by orange lines. The distance distribution of the undocked Eg5 NL in the presence of ADP is indicated by blue line in *D*.

**ATP-Induced Structural Transitions in the NL and Switch-1 Can Be Observed Using ($TR^2$)-FRET.** We examined ATP-induced changes in distances between the donor and acceptor probes in our four constructs by means of $(TR)^2$-FRET (20, 26, 27), acquiring time-resolved fluorescence waveforms of donor and donor/acceptor-labeled samples every 100 μs after mixing with ATP. Because ATP binding to kinesin-1 at physiological concentrations of nucleotide is ∼1,800 $s^{-1}$ at room temperature (28, 29), we performed all of our experiments at 10 °C so we could accurately measure the kinetics of nucleotide-induced changes in the NL and switch-1. Representative waveforms after mixing with 2 mM ATP are depicted for $Kin1_{NL}$:MT and $Kin1_{Sw1}$:MT in Fig. 2 *A* and *B* and for $Eg5_{NL}$:MT and $Eg5_{Sw1}$:MT in Fig. 3 *A* and *B*, respectively. We determined how $F_D$, the total fluorescence of the donor-labeled motor, and $F_{DA}$, the total fluorescence of donor/acceptor labeled motor, change during ATP binding. Results produced by mixing labeled motor:MT complexes with 2 mM ATP are depicted for $F_D$ in *SI Appendix*, Fig. S3 and for $F_{DA}$ in Fig. 2 *C* and *D* (red) for kinesin-1 and Fig. 3 *C* and *D* (red) for Eg5. After mixing with ATP, $F_{DA}$ for each of the four constructs changes significantly although $F_D$ does not, implying that ATP binding and hydrolysis do not affect the donor quantum yield. The value of $F_{DA}$ is sensitive to the relative orientation of the donor and acceptor dipoles, represented by the term $\kappa^2$ (21). This term becomes problematic when the donor and acceptor probes are rigidly oriented. However, the anisotropies and rotational correlation times of the AEDANS donor for all four constructs are consistent with large-amplitude probe dynamics in the nanosecond time scale, and they do not change with ATP or MT binding (*SI Appendix*, Table S4). This finding confirms that the changes in $F_{DA}$ reflect corresponding changes in interprobe distances (21).

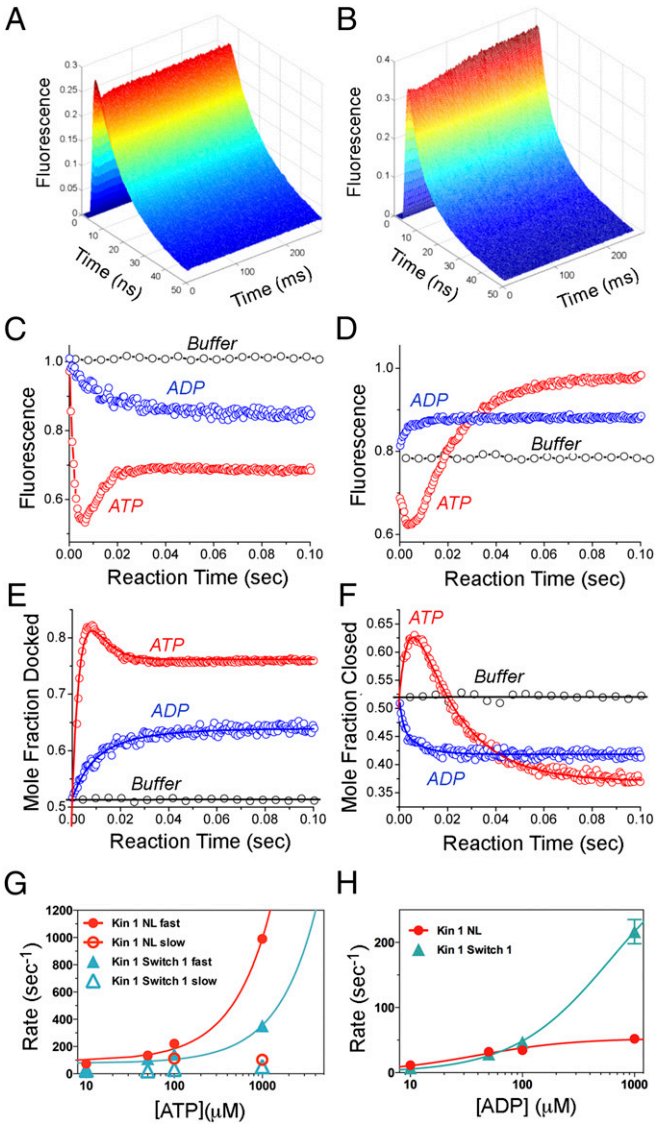


**Fig. 2.** Transient time-resolved FRET during ATP binding to rigor MT bound kinesin-1. (*A* and *B*) Representative waveforms after mixing 2 mM ATP with 1 μM AEDANS/DDPM-labeled $Kin1_{NL}$ (*A*) or $Kin1_{sw1}$ (*B*) bound to 2 μM MTs. (*C* and *D*) Relative total fluorescence of $Kin1_{NL}$ (*C*) or $Kin1_{sw1}$ (*D*) showing magnitude and direction of change in AEDANS fluorescence for MT bound samples mixed with buffer (black), 2 mM ATP (red), or 2 mM ADP (blue). (*E* and *F*) Mole fraction of docked NL (*E*) or closed switch-1 (*F*) for MT bound Kin1 samples after mixing with 2 mM ATP (red) or 2 mM ADP (blue). (*G*) Linear plot of rate constant versus [ATP] for the two phases illustrated in the red transients in *E* and *F* on a semilog scale. The plots for $Kin1_{NL}$ are colored red, and those for $Kin1_{sw1}$ are colored cyan. Apparent second order rate constants for the faster phases and mean rate constants for the slower phases are summarized in Table 1. (*H*) Hyperbolic plot of rate constant versus [ADP] for the single phase illustrated in the blue transients in *E* and *F* on a semilog scale. The rate versus [ADP] curve for $Kin1_{NL}$ is in red, and that for $Kin1_{sw1}$ in cyan. Extrapolated maximum rate constants are summarized in Table 1. Conditions: 25 mM Hepes, pH 7.50, 50 mM potassium acetate, 5 mM magnesium acetate, 1 mM EGTA, 10 °C. $n$ = 3–6.

**Analyzing the $(TR)^2$-FRET Waveforms Reveals That both the NL and Switch-1 Assume Two Conformations with Mole Fractions that Change with ATP Binding and Hydrolysis.** We analyzed the $(TR)^2$-FRET data by assuming that any time-dependent changes in the waveforms (Figs. 2 *A* and *B* and 3 *A* and *B*) and in the resulting values of $F_{DA}$ (Figs. 2 *C* and *D* and 3 *C* and *D*) correspond to changes in the mole fractions of the NL and switch-1 orientations, as justified by our prior studies (20, 27, 30–33). We simultaneously fit the fluorescence decays of donor and donor/acceptor-labeled constructs and optimized the model parameters to determine the number of structures detected by assuming Gaussian distributions for the interprobe distances and the center and width of these distance distributions. The best fit of the data showed that both the NL and switch-1 assume two distinct conformations (Fig. 1 and *SI Appendix*, Table S5) that are consistent with structural models of docked and undocked NL and open (ADP-like) and closed (ATP-like) switch-1.

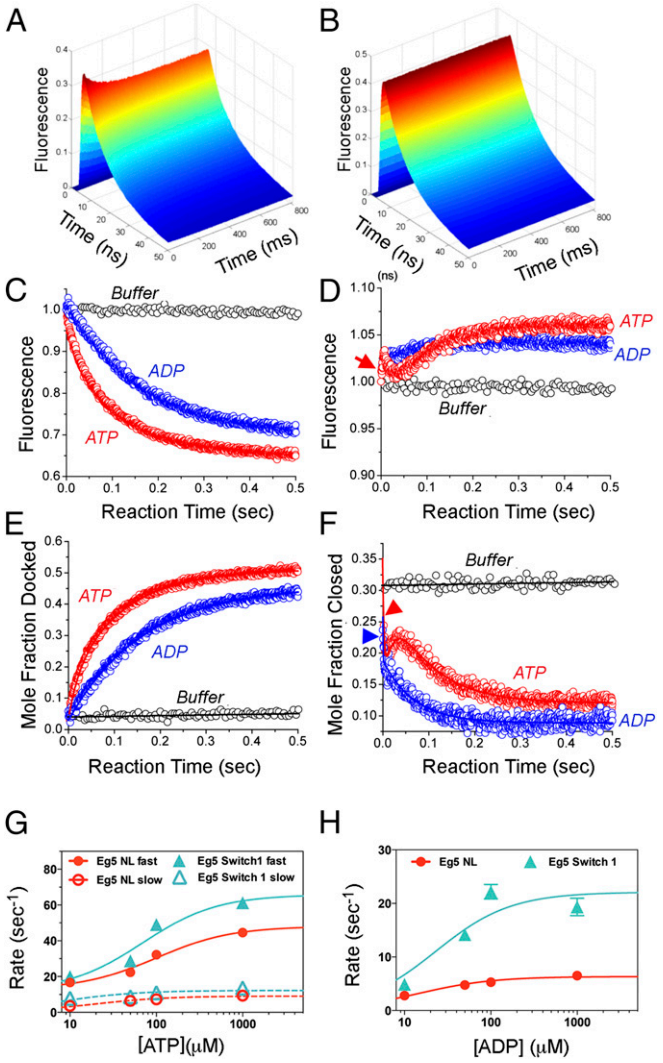


**Fig. 3.** Transient time-resolved FRET during ATP binding to rigor MT bound Eg5. (*A* and *B*) Representative waveforms ($n$ = 3–6) after mixing 2 mM ATP with 1 μM AEDANS + DDPM labeled $Eg5_{NL}$ (*A*) or $Eg5_{sw1}$ (*B*) bound to 2 μM MTs. (*C* and *D*) Relative total fluorescence of $Eg5_{NL}$ (*C*) or $Eg5_{sw1}$ (*D*) showing magnitude and direction of change in AEDANS fluorescence for MT bound samples mixed with buffer (black), 1 mM ATP (red), or 1 mM ADP (blue). (*E* and *F*) Mole fraction of docked NL (*E*) or closed switch-1 (*F*) for MT bound Eg5 samples after mixing with 2 mM ATP (red) or 2 mM ADP (blue). Data from *D* and *F* are replotted in *SI Appendix*, Fig. S4 over a shorter time window to more clearly show the initial stages in the $Eg5_{sw1}$ transients. (*G*) Hyperbolic plot of rate constant versus [ATP] for the two phases illustrated in the red transients in *E* and *F* on a linear scale. The plots for $Eg5_{NL}$ are colored red, and those for $Eg5_{sw1}$ are colored cyan. Extrapolated maximum rate constants are summarized in Table 2. (*H*) Hyperbolic plot of rate constant versus [ADP] for the single phase illustrated in the blue transients in *E* and *F* on a linear scale. The rate versus [ADP] curve for $Eg5_{NL}$ is in red, and that for $Eg5_{sw1}$ in cyan. Extrapolated maximum rate constants are summarized in Table 2. Conditions as in Fig. 2.

**Table 1. Mole fractions, apparent $K_{eq}$, and rate constants of NL docking and switch-1 closure for kinesin-1 at 10 °C measured by $(TR^2)$FRET**

| Sample | Mixed with | Phase | Rate constant | Mole fraction docked or closed | $K_{eq(App)}$ |
|---|---|---|---|---|---|
| Mole fraction docked | | | | | |
| Rigor $Kin1_{NL}$:MT | Buffer | — | — | 0.51 | 1.04 |
| Rigor $Kin1_{NL}$:MT | ATP | 1 | $0.90 \pm 0.04\ \mu M^{-1}\ s^{-1}$ | 0.81 | 4.26 |
| Rigor $Kin1_{NL}$:MT | ATP | 2 | $104.7 \pm 23\ s^{-1}$ | 0.76 | 3.17 |
| Rigor $Kin1_{NL}$:MT | ADP | — | $52.7 \pm 3.4\ s^{-1}$ | 0.60 | 1.50 |
| Mole fraction closed | | | | | |
| Rigor $Kin1_{Sw1}$:MT | Buffer | — | — | 0.52 | 1.08 |
| Rigor $Kin1_{Sw1}$:MT | ATP | 1 | $0.28 \pm 0.06\ \mu M^{-1}\ s^{-1}$ | 0.63 | 1.7 |
| Rigor $Kin1_{Sw1}$:MT | ATP | 2 | $50.0 \pm 13.8\ s^{-1}$ | 0.37 | 0.59 |
| Rigor $Kin1_{Sw1}$:MT | ADP | — | $351.7 \pm 15.2\ s^{-1}$ | 0.42 | 0.72 |

Alternative models that assumed a larger or smaller number of structures are either not consistent with the data or fail to improve the $\chi^2$ of the fit (*SI Appendix*, Fig. S5).

We verified that fitting our data to a set of global distance distribution parameters did not change the result of the fitting, by analyzing representative TR-FRET datasets independently (*SI Appendix*, Fig. S9). This analysis showed that the global constraint improves the certainty of fitting because multiple orthogonal datasets are evaluated simultaneously, but that even when these same datasets are fit independently, the interpretation of the data does not change. TR-FRET detects two structural states of the NL and switch-1 in both kinesin-1 and Eg5 and these states are consistent with predictions based on available high-resolution crystal and cryo-EM structures.

An advantage of the $(TR)^2$-FRET approach is that it allows us to measure both the changes in the mole fraction of docked NL and closed switch-1, as well as the kinetics of these changes with nucleotide binding. By correlating the one with the other, we can identify the biochemical transitions that are likely responsible for the observed structural transitions. All four of the constructs used in this study were designed so that $F_{DA}$ decreases when the mole fraction of docked NL (for $Kin1_{NL}$ and $Eg5_{NL}$) and closed switch-1 (for $Kin1_{Sw1}$ and $Eg5_{Sw1}$) increase. Mixing $Kin1_{NL}$ and $Kin1_{Sw1}$ with ATP initially increases the mole fractions of both docked NL and closed switch-1 (Fig. 2 *E* and *F*), and the kinetics of these conformational transitions (Fig. 2*G* and Table 1) imply that they occur with ATP binding (8). The kinetics of the subsequent declines in docked NL and closed switch-1 are consistent with ATP hydrolysis (Fig. 3*G* and Table 1). In contrast, mixing $Eg5_{NL}$ with ATP increases the mole fraction of docked NL in two sequential steps (Fig. 3*E*). The kinetics of the first step are consistent with ATP binding, and that for the second are consistent with ATP hydrolysis (Fig. 3*G* and Table 2). For $Eg5_{Sw1}$, the kinetics are more complex, with a rapid initial fall in the mole fraction of closed switch-1 (Fig. 3*F*, red arrowhead) followed by a rise and then subsequent fall. The kinetics of the latter rising and final falling phases imply that switch-1 closes with ATP binding and reopens with hydrolysis (Fig. 3*G* and Table 2). However, the initial rapid decrease in the mole fraction of switch-1 suggests that there is a rapid shift in the [closed]/[open] equilibrium that precedes ATP binding.

The mole fractions of docked NL and closed switch-1 for a nucleotide-free (rigor) kinesin-1:MT complex are both ~50% at 10 °C (Fig. 2 *E* and *F*, black, and Table 1), and after mixing with ATP, both increase. However, after about 5–10 ms—the time course for ATP hydrolysis—they diverge somewhat, with the mole fraction of closed switch-1 decreasing more than that for docked NL. This finding can be appreciated by plotting the ratio of the mole fraction of docked NL to closed switch-1 versus time after mixing with ATP (Fig. 4*A*, red trace) versus buffer (Fig. 4*A*, black trace). In rigor, this is close to 1.0, suggesting that these conformational equilibria are linked together and remain so until ATP hydrolysis. Fig. 3 *E* and *F* and Table 2 demonstrate the corresponding changes in Eg5. Unlike kinesin-1, the conformational equilibria of the NL and switch-1 do not appear to be linked together. The mole fraction of docked NL in rigor is quite small (4%) but an appreciable fraction of switch-1 is closed (31%). Through the course of ATP binding and hydrolysis, this ratio reverses, with a much greater mole fraction of docked NL to closed switch-1 (Fig. 4*B*, red trace).

The relatively large fraction of docked NL in rigor for a MT:$Kin1_{NL}$ complex stands in contrast to a generally accepted consensus model (4, 5, 34), which argues that the NL is disordered in rigor on the MT. However, we have performed our kinetic experiments at 10 °C to slow the rates for kinesin-1 so we could accurately measure the kinetics, and it is a priori unclear how a

**Table 2. Mole fractions, apparent $K_{eq}$, and rate constants of NL docking and switch-1 closure for Eg5 at 10 °C**

| Sample | Mixed with | Phase | Rate constant | Mole fraction docked or closed | $K_{eq(App)}$ |
|---|---|---|---|---|---|
| Mole fraction docked | | | | | |
| Rigor $Eg5_{NL}$:MT | Buffer | — | — | 0.04 | 0.04 |
| Rigor $Eg5_{NL}$:MT | ATP | 1 | $35.2 \pm 4.9\ s^{-1}$ | 0.15 | 0.18 |
| Rigor $Eg5_{NL}$:MT | ATP | 2 | $9.1 \pm 0.5\ s^{-1}$ | 0.51 | 1.04 |
| Rigor $Eg5_{NL}$:MT | ADP | — | $6.3 \pm 0.2\ s^{-1}$ | 0.66 | 1.94 |
| Mole fraction closed | | | | | |
| Rigor $Eg5_{Sw1}$:MT | Buffer | — | — | 0.31 | 0.45 |
| Rigor $Eg5_{Sw1}$:MT | ATP | 1 | $360 \pm 84\ s^{-1}$ | 0.12 | 0.14 |
| Rigor $Eg5_{Sw1}$:MT | ATP | 2 | $54.0 \pm 14.1\ s^{-1}$ | 0.31 | 0.45 |
| Rigor $Eg5_{Sw1}$:MT | ATP | 3 | $12.2 \pm 1.4\ s^{-1}$ | 0.12 | 0.14 |
| Rigor $Eg5_{Sw1}$:MT | ADP | — | $22.1 \pm 3.6\ s^{-1}$ | 0.09 | 0.10 |

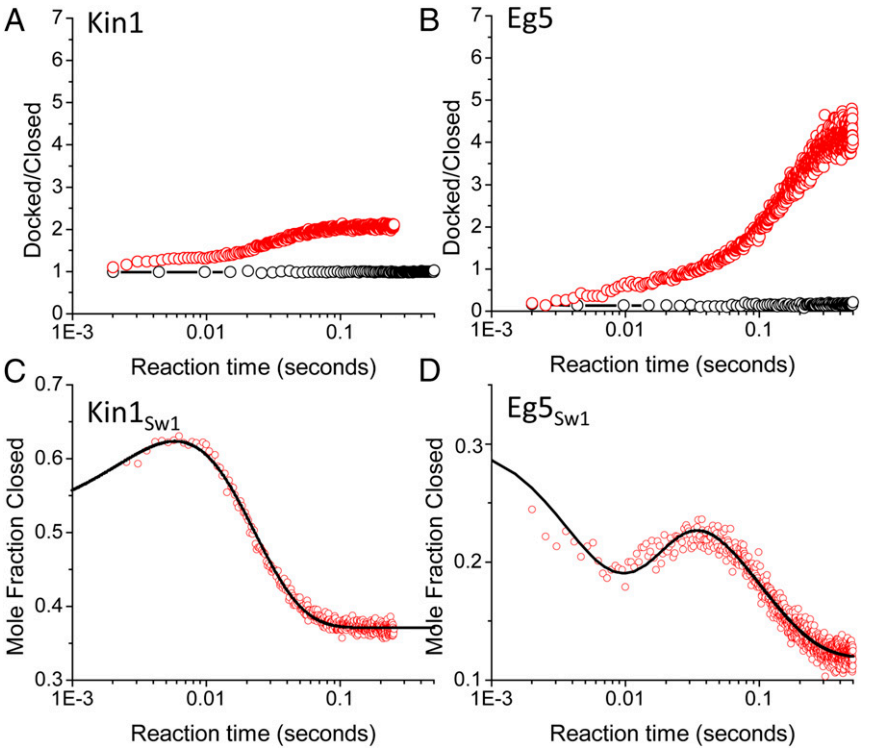


**Fig. 4.** Transient changes in apparent NL/Switch-1 coupling. (*A* and *B*) The ratio of mole fraction of docked NL to mole fraction of closed switch-1 versus time after mixing with buffer (black) or 2 mM ATP (red). For kinesin-1 (*A*), the ratio is close to unity before mixing and remains so for the first 10 ms after mixing. For Eg5 (*B*), the ratio starts at 0.13 in rigor and continually increases after mixing with ATP. (*C* and *D*) Simulated transient changes in the mole fraction of the closed switch-1 structural state (black line) fit to the measured mole fraction (red symbols) in $Kin1_{Sw1}$ (*C*) or $Eg5_{Sw1}$ (*D*).

docked/undocked equilibrium, as measured by FRET, is affected by raising the temperature to a more physiologically relevant range. We therefore used TR-FRET to measure the mole fraction of docked NL for MT:$Kin1_{NL}$ and MT:$Eg5_{NL}$ complexes as a function of temperature, and results are depicted in *SI Appendix*, Fig. S8 in the absence of nucleotide (*SI Appendix*, Fig. S8, black) and in the presence of 1 mM AMPPNP (*SI Appendix*, Fig. S8, magenta). Results are depicted on a linear scale (*SI Appendix*, Fig. S8, mole fraction docked NL versus temperature) for $Kin1_{NL}$ in *SI Appendix*, Fig. S8*A* and for $Eg5_{NL}$ in *SI Appendix*, Fig. S8*C*, and according to the van't Hoff equation for $Kin1_{NL}$ in *SI Appendix*, Fig. S8*B* and for $Eg5_{NL}$ in *SI Appendix*, Fig. S8*D*. The derived values for ΔH and TΔS are summarized in *SI Appendix*, Table S9. Two points are apparent from these data. First, as expected, AMPPNP induces near complete NL docking for both kinesin-1 and Eg5. Although our values of ΔH and TΔS are different from those published previously for kinesin-1 (22), we also note that this prior work calculated an equilibrium constant for NL docking from changes in the mobility of an EPR spin probe, whereas our study uses the more directly interpretable distance-sensitive FRET approach. Nevertheless, the free energies that can be calculated from *SI Appendix*, Table S9 do indeed show, consistent with the consensus model, that NL docking is more favorable energetically in the presence of AMPPNP than it is in rigor. Second, our data also clearly demonstrate that the large mole fraction of docked NL we see in a rigor MT:kinesin-1 complex is a direct effect of the lower temperature that we have used in this study, and that this mole fraction approaches zero in a more physiologically relevant temperature range.

**Binding of ADP Enhances NL Docking but Reduces Switch-1 Closure.** We repeated these experiments by mixing with ADP, and the results are depicted in Figs. 2 and 3 in the blue traces at a final [ADP] of 1 mM. Fitting the waveforms to a structure-based FRET model reveals that for kinesin-1, the center and width of the modeled interprobe distance distributions with ADP are indistinguishable from those with ATP (Fig. 1 *C* and *E* and tabulated in *SI Appendix*, Table S5). ATP and ADP similarly produce identical interprobe distances for $Eg5_{Sw1}$ (Fig. 1 *D* and *F* and tabulated in *SI Appendix*, Table S5). However, the distance distribution of the undocked NL in a MT-bound, $Eg5_{NL}$:ADP complex is 1-nm closer to the β7 strand than that for the undocked orientation in ATP (Fig. 1*D*, blue, and *SI Appendix*, Table S5), consistent with the crystallographic structure of Eg5:ADP (19). ADP binding substantially increases the mole fraction of docked NL in Eg5, compared with kinesin-1. It also decreases the mole fraction of closed switch-1 in both Eg5 and kinesin-1. These changes in the NL and switch-1 are monophasic except for $Eg5_{Sw1}$, where, similar to the case for ATP, a fast initial decrease in the mole fraction of closed switch-1 can be observed (Fig. 3*F*, blue arrowhead). The rate constant for a single exponential fit (or in the case of $Eg5_{Sw1}$ at 1 mM ADP, the slower phase of a double exponential fit) varies hyperbolically with [ADP] (Figs. 2*H* and 3*H*), defining maximum rates summarized in Tables 1 and 2. For both constructs, the rates of NL docking and MT dissociation are similar to each other and are ∼four- to sevenfold slower than that for switch-1 opening (8, 16), suggesting that ADP-induced changes in MT affinity occur hand-in-hand with corresponding changes in the state of the NL but not with the state of switch-1.

**Modeling of the $(TR^2)$-FRET Transients Suggests That the Kinetics of ATP Binding Are Controlled by Different Mechanisms in Kinesin-1 and Eg5.** To gain insight into how the structural changes detected by $(TR)^2$-FRET correspond to the known biochemical transitions in the ATPase cycle of kinesins, we simulated the temporal changes in the mole fraction of closed switch-1 using *KinTek Explorer* by

applying the following model constraints for both kinesin-1 and Eg5: (*i*) the closed and open conformations of switch-1 are both populated in rigor and the equilibrium constant, defined as [closed]/[open], is 1.08 for kinesin-1 and 0.45 for Eg5 (Tables 1 and 2); (*ii*) ATP can only bind to the open state, and does so very rapidly (>>1,000 $s^{-1}$) for both Eg5 and kinesin-1; and (*iii*) ATP hydrolysis requires switch-1 to close. These assumptions are incorporated into the kinetic scheme shown in Fig. 5, where M stands for the microtubule-bound kinesin motor domain, the subscripts C and O stand for closed and open switch-1 conformations, respectively, T is ATP, D is ADP, and $P_i$ is inorganic phosphate. These simulations were performed by assigning values to $K_{ATP}•k_2$ and $k_{-2}$, the rate constants for the ATP binding step, derived from previous measurements using the ATP analog 2′ deoxy 3′ mant ATP [2′dmT (8, 16)], which produces a fluorescence enhancement when it binds to kinesins. The resulting fits are illustrated in Fig. 4*C* (for $Kin1_{Sw1}$) and Fig. 4*D* (for $Eg5_{Sw1}$), where the open red circles are the data from Figs. 2*F* and 3*F*, and the black curves are simulations from *KinTek Explorer*. These simulations yielded values for the rate constants in Scheme 1 (Fig. 5) that are summarized in *SI Appendix*, Table S8. What the values show is that the initial switch-1 isomerization ($k_1/k_{-1}$) is rapid for both Eg5 and kinesin-1, and in kinesin-1, it controls the rate at which ATP can bind. However, the rate of 2′ dmT binding to Eg5 is much slower than it is for kinesin-1, suggesting that some other structure besides switch-1 is gating the ATP binding step in Eg5. As we will discuss below, we propose that this structure is L5.

**Disrupting an Interaction Between L5 and α3 in Eg5 Accelerates ATP Binding.** Switch-1 in a rigor Eg5:MT complex is largely open. If ATP could rapidly bind to the open conformation of switch-1, we would predict that the rate of ATP binding to the Eg5:MT complex should be similar to that for kinesin-1. However, as noted above, this is not the case because binding of 2′dmT, NL docking, and switch-1 closure (Table 2) all occur at about the same rate, which is ∼20-fold slower than for kinesin-1. One explanation is that some other structure is gating these processes in Eg5, and several lines of evidence suggest that this is loop L5. We had previously proposed (12, 17, 35) that in Eg5, L5 acts as a conformational latch that sterically blocks ATP binding through a reversible interaction with helix α3. This interaction is stabilized in part by hydrophobic ring stacking between W127 in L5 and Y211 in α3 (19). We therefore used a previously described Eg5 construct (35) that has a single reactive cysteine, which replaces W127 ($Eg5_{W127C}$). We measured the kinetics of 2′dmT binding to this construct and compared our results to those where we move this cysteine one residue over ($Eg5_{T126C}$). Both constructs produce a biphasic rise in fluorescence (Fig. 6*A* for $Eg5_{W127C}$ and Fig. 6*B* for $Eg5_{T126C}$), with the rate constant for the faster phase varying linearly with [2′dmT] for both (Fig. 6*C*, solid points and lines). However, the apparent second-order rate constant for this phase for $Eg5_{W127C}$ (6.3 ± 0.9 $\mu M^{-1}/s^{-1}$) is over 20-fold greater than that for $Eg5_{T126C}$ (0.3 ± 0.06 $\mu M^{-1}/s^{-1}$). A previous cryo-EM study proposed that in rigor, a portion of L5 is in a position that would sterically block ATP binding (12). Our results now suggest that the W127–Y211 interaction stabilizes this blocking conformation of L5, and disrupting it makes L5 more flexible, accelerating both its movement away from the catalytic site and subsequent ATP binding.

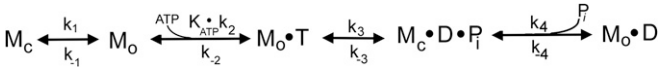


**Fig. 5.** Kinetic scheme.

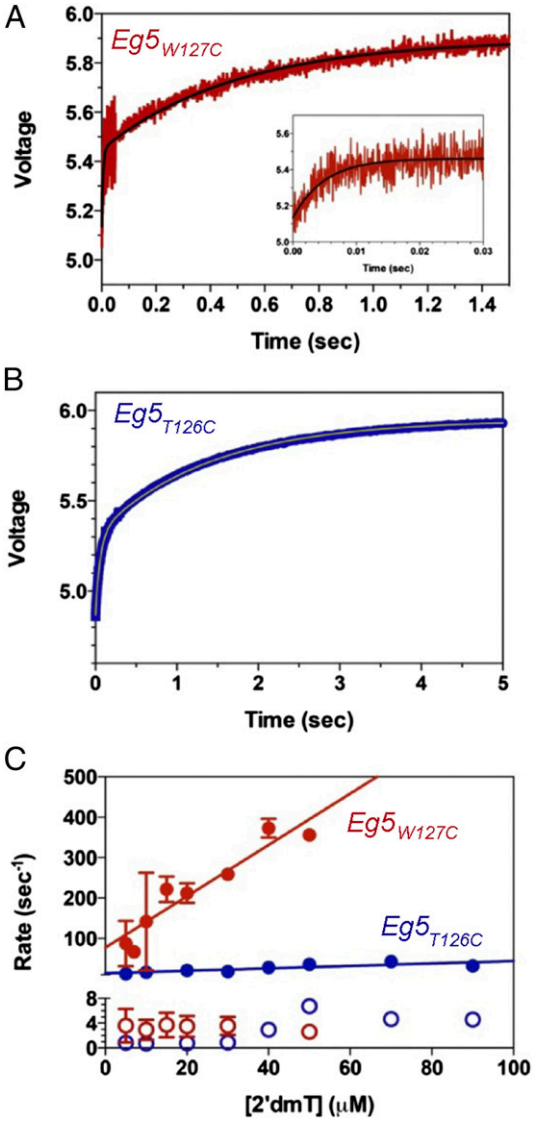


**Fig. 6.** Disrupting the L5-α3 interaction accelerates ATP binding to Eg5. (*A*) An $Eg5_{W125C}$:MT complex was mixed in the stopped flow with 60 μM 2′dmT, and the fluorescence enhancement of the mant fluorophore was monitored by FRET from MT tryptophans. The resulting transient (jagged red curve) consists of two phases that could be fit to a double exponential rate equation (solid black curve). (*Inset*) The initial rapid phase on an expanded *x* axis. (*B*) The corresponding experiment with a $Eg5_{T126C}$:MT complex also demonstrates a biphasic transient. (*C*) Plot of the rate constants for $Eg5_{W125C}$ (red) and $Eg5_{T126C}$ (blue) versus [2′dmT] for the first phase (solid circles and lines) and second phase (open circles). The apparent second order rate constant for the faster phase is more than 20-fold greater for $Eg5_{W127C}$ than for $Eg5_{T126C}$.

## Discussion

**$(TR)^2$-FRET Can Provide Information on the Kinetics of Nucleotide-Induced Changes in the NL and of Switch-1.** A generally accepted model has proposed that the NL of MT-bound kinesin alternates between two states—one that is oriented toward the plus end of the MT and docked along the motor core, and one which is undocked and disordered (5)—with ATP binding favoring a disordered-to-docked transition. Much of the evidence in support of this model has come from EPR-based studies, in which reduction in probe mobility has been taken as a spectroscopic signature of the docked state (5, 22). Predictions based on these spectroscopic findings are consistent with crystallographic and

cryo-EM structural studies in the case of kinesin-1 (6, 15, 34, 36). However, in the case of Eg5, a reduction in NL EPR probe mobility that was seen with ADP release led to the suggestion that this step represents the "power stroke"—the step in the mechanochemical cycle when NL docking occurs (37). However, this conclusion is at odds with cryo-EM reconstructions of rigor Eg5:MT complexes, which show that although the NL in rigor is less mobile than in ADP, the orientations of the NL in these two states are very similar (7). Thus, alterations in probe mobility may not be a consistent surrogate marker for NL docking across different kinesins with different functions.

Part of the problem is that the methods used so far do not provide robust measures of how many orientations the NL and switch-1 assume in different nucleotide states, let alone how they change during transient biochemical conditions. This is illustrated by $(TR)^2$-FRET studies of the myosin II motor domain (20, 27), which demonstrate that ATP binding induces a bending of the switch-2 helix; that in the steady-state this helix assumes an equilibrium distribution of both bent and straight orientations; and that there is a rapid equilibration of bent and straight orientations of this helix that precedes actin-activated phosphate release (20). These studies highlight the unique ability of $(TR)^2$-FRET to investigate how biochemical and structural transitions are coordinated together. We therefore sought to re-examine the process of nucleotide-induced orientation changes, not only in the NL but also in switch-1, by applying this temporal- and distance-sensitive spectroscopic approach to kinesin-1 and Eg5.

**Nucleotide Binding Shifts the NL Conformational Equilibrium Toward the Docked Orientation to Differing Degrees in Kinesin-1 and Eg5.** Overall, our results with donor/acceptor $Kin1_{NL}$ are consistent with previous spectroscopic studies (5, 22, 34). We too find that ATP binding induces an increase in the mole fraction of NL docking, with kinetics consistent with our earlier studies (8), although $(TR)^2$-FRET now also enables us to see that a substantial fraction remains docked even after a subsequent step, corresponding kinetically to ATP hydrolysis (8). We also find that both rigor and ADP-bound $Kin1_{NL}$:MT complexes still have a substantial mole fraction of docked NL. As we have shown, this reflects the effect of the lower temperature we needed to use to observe the relevant kinetics (10 °C). This effect of temperature on NL docking may also provide an explanation for cryo-EM reconstructions of dimeric kinesin-1:MT complexes, which show the tethered head positioned in a forward orientation (38). ADP docks the NL of a $Kin1_{NL}$:MT complex at 10 °C to a lesser degree than does ATP, and with kinetics consistent with formation of a weak binding state (Table 1). Although this effect with ADP would be considerably smaller at physiologic temperature, even a modest tendency for the NL to dock while the MT-attached motor has ADP in its catalytic site may provide some degree of "safety" for a highly processive transport motor. This arrangement would tend to position the tethered head in a forward orientation and enhance its chances to securely attach to the next tubulin dimer before the weakly bound, ADP-containing rear head falls off.

The corresponding situation is different for $Eg5_{NL}$ (Fig. 3 and Table 2). ATP binding to an Eg5:MT complex favors NL docking. However, unlike kinesin-1, nearly all of the NLs in a rigor Eg5:MT complex are undocked at 10 °C. Furthermore, ATP and ADP both induce NL docking in Eg5, and to a similar degree. In the case of ATP, NL docking occurs in two steps associated with rates consistent with ATP binding and hydrolysis (Table 2), whereas with ADP, the kinetics of NL docking are consistent with formation of a weak-binding state (Table 2) at 10 °C. Our finding that ADP binding induces NL docking in the Eg5:MT complex is not simply a consequence of the lower temperature used in our present study, because we had previously shown that mixing ADP with a donor/acceptor-labeled $Eg5_{NL}$:MT complex at room temperature also produces FRET changes consistent with NL docking (12). As with kinesin-1, having the NL of MT-attached Eg5 remain docked even after hydrolysis provides a degree of safety. This is particularly an issue with Eg5, because hydrolysis at $\sim 12\ s^{-1}$ is only four to five times slower than NL docking, whereas in kinesin-1 this difference is >10-fold (29, 39).

**ATP Binding Shifts Switch-1 Toward the Closed State, Whereas ATP Hydrolysis and ADP Binding Shifts It Back Toward the Open State.** A recent crystallographic study has proposed that switch-1 closure is necessary for ATP hydrolysis (19). This leads to two predictions. First, the mole fraction of closed switch-1 should initially increase following ATP binding, as the system prepares to hydrolyze bound ATP, and should then decrease after hydrolysis and $P_i$ release. Second, ADP binding should favor the open switch-1 conformation, as seen in the crystallographic model of kinesin-1:ADP (2). We observe both of these predictions for $Kin1_{Sw1}$ (Fig. 2 and Table 1). For kinesin-1, the apparent second-order rate constant for switch-1 closure is over threefold slower than for NL docking (Fig. 2*G* and Table 1), suggesting that NL docking precedes and may be required for switch-1 to close into a hydrolysis-competent state. Because monomeric kinesin-1 cannot generate intramolecular strain, this result supports our earlier proposal that NL position, and not intramolecular strain per se, regulates ATP hydrolysis through its effects on the switch-1 conformational equilibrium (11). Because ATP hydrolysis for kinesin-1 is reversible (40), the kinesin-1:ATP biochemical state would transiently accumulate, consistent with the initial lag in Fig. 4*A* (red), and because kinesin-1:ADP-$P_i$ is strongly bound to the MT (41), the NL would remain largely docked after hydrolysis, while switch-1 would reopen, accounting for the moderate increase in the molar ratio of docked NL to closed switch-1 (Fig. 4*A*). All in all, the data for our kinesin-1 constructs suggest that the conformations of the NL and switch-1 are tightly coordinated in the strong binding states. For a processively moving motor like kinesin-1 to remain attached to the MT while moving forward, the catalytic domains must balance the need to bind strongly to the MT lattice with the need to let go to keep from freezing in one position. This requires that ATP binding to the attached head in a dimeric motor needs to not only induce forward movement of the tethered head but also set in motion a sequence of steps that leads to ATP hydrolysis and subsequent formation of a weak-binding state. NL docking is required for the former, and switch-1 closure appears to be required for the latter (10), and our results in Fig. 4*A* support this temporal linkage between the states of these two important domains in kinesin-1. A major difference between kinesin-1 and Eg5 is in the degree of linkage between the states of the NL and of switch-1. The results summarized in Table 2 and depicted in Fig. 4*B* for Eg5 indicate that, unlike the case for kinesin-1, an ATP-induced increase in NL docking does not go hand-in-hand with a proportional increase in switch-1 closure. This would generate a system where Eg5 motors would tend to remain strongly bound for a significant time after the power stroke, a feature that might allow this motor to generate sustained force in opposition to loads imposed by dynein and ncd.

**Differences in the Structural Kinetics of Kinesin-1 and Eg5 Provide Mechanistic Insight into How the Different Physiologies of these Motors Shape Differences in Their Enzymologies.** Our data in Fig. 6 argue that in Eg5, the kinetics of the L5–α3 interaction regulate the corresponding kinetics of ATP binding and subsequent switch-1 closure, and NL docking. Why does Eg5 use this mechanism of gating when kinesin-1 relies on NL position? As a highly processive transport motor, kinesin-1 must ensure that its two motor domains remain out of phase enzymatically to keep both from simultaneously populating a weak MT binding state and dissociating. It spends an appreciable amount of its cycle with both motor domains bound to the MT, a state that would automatically enforce a docked NL orientation in one motor and

an undocked in the other. Thus, a mechanism that relies on NL position to gate ATP hydrolysis would fit naturally into this motor's hand-over-hand stepping mechanism. In contrast, Eg5 is a poorly processive motor (25), likely because of its longer and more flexible NL (42). This enhanced flexibility might prevent gating of the Eg5 ATPase through a NL position-sensitive mechanism and could explain how both heads of dimeric Eg5 constructs can bind to MTs in rigor (43). Without any other gating mechanism, ATP binding to Eg5 would be very rapid, and with the ATPase equilibrium favoring the ADP-$P_i$ state, a large fraction of motors could assume a weak-binding conformation with $P_i$ release and dissociate. Kinetically regulating NL docking and switch-1 closure by tying both to a rate-limiting conformational change in L5 could slow both processes and further enhance the fraction of Eg5, with both motor domains strongly bound in rigor to the MT. Finally, the tight coupling between docked NL and closed switch-1 conformations in rigor kinesin-1 would tend to minimize any back stepping in the presence of opposing force. This is because forced undocking of the NL in a rigor motor would be expected to likewise force switch-1 into an open, hydrolysis-incompetent conformation. This head would therefore remain strongly attached and would resist the dissociation needed for backward stepping.

Finally, the $(TR)^2$-FRET studies we have reported here have been limited to monomeric kinesin constructs that operate in the absence of mechanical load or intramolecular strain. However, the methodologies we have used here are readily applicable to the more complicated but physiologically relevant higher-order dimers and tetramers that function within cells.

## Materials and Methods

A complete discussion of all methods, including generation of the kinesin cysteine mutants, expression, purification, ATPase assays, transient kinetic methodologies, and $(TR^2)$-FRET data acquisition and analysis is included in the *SI Appendix, Materials and Methods*.

**ACKNOWLEDGMENTS.** This work was supported by National Institutes of Health Grants GM102875 and NS073610 (to S.S.R.), and AR32961 (to D.D. T.); and American Heart Association Grant 14SDG20480032 (to J.M.M.). Time-resolved fluorescence experiments were performed in the University of Minnesota Biophysical Spectroscopy Center. Matlab-based data analysis was performed at the Minnesota Super Computing Institute.

1. Rath O, Kozielski F (2012) Kinesins and cancer. *Nat Rev Cancer* 12(8):527–539.
2. Kull FJ, Sablin EP, Lau R, Fletterick RJ, Vale RD (1996) Crystal structure of the kinesin motor domain reveals a structural similarity to myosin. *Nature* 380(6574):550–555.
3. Sablin EP, Kull FJ, Cooke R, Vale RD, Fletterick RJ (1996) Crystal structure of the motor domain of the kinesin-related motor ncd. *Nature* 380(6574):555–559.
4. Vale RD, Milligan RA (2000) The way things move: Looking under the hood of molecular motor proteins. *Science* 288(5463):88–95.
5. Rice S, et al. (1999) A structural change in the kinesin motor protein that drives motility. *Nature* 402(6763):778–784.
6. Gigant B, et al. (2013) Structure of a kinesin–tubulin complex and implications for kinesin motility. *Nat Struct Mol Biol* 20(8):1001–1007.
7. Goulet A, et al. (2014) Comprehensive structural model of the mechanochemical cycle of a mitotic motor highlights molecular adaptations in the kinesin family. *Proc Natl Acad Sci USA* 111(5):1837–1842.
8. Rosenfeld SS, Jefferson GM, King PH (2001) ATP reorients the neck linker of kinesin in two sequential steps. *J Biol Chem* 276(43):40167–40174.
9. Shang Z, et al. (2014) High-resolution structures of kinesin on microtubules provide a basis for nucleotide-gated force-generation. *eLife* 3:e04686.
10. Cao L, et al. (2014) The structure of apo-kinesin bound to tubulin links the nucleotide cycle to movement. *Nat Commun* 5:5364.
11. Clancy BE, Behnke-Parks WM, Andreasson JOL, Rosenfeld SS, Block SM (2011) A universal pathway for kinesin stepping. *Nat Struct Mol Biol* 18(9):1020–1027.
12. Goulet A, et al. (2012) The structural basis of force generation by the mitotic motor kinesin-5. *J Biol Chem* 287(53):44654–44666.
13. Sindelar CV (2011) A seesaw model for intermolecular gating in the kinesin motor protein. *Biophys Rev* 3(2):85–100.
14. Cross RA (2004) The kinetic mechanism of kinesin. *Trends Biochem Sci* 29(6):301–309.
15. Sindelar CV, Downing KH (2007) The beginning of kinesin's force-generating cycle visualized at 9-A resolution. *J Cell Biol* 177(3):377–385.
16. Rosenfeld SS, Xing J, Jefferson GM, King PH (2005) Docking and rolling, a model of how the mitotic motor Eg5 works. *J Biol Chem* 280(42):35684–35695.
17. Behnke-Parks WM, et al. (2011) Loop L5 acts as a conformational latch in the mitotic kinesin Eg5. *J Biol Chem* 286(7):5242–5253.
18. Parke CL, Wojcik EJ, Kim S, Worthylake DK (2010) ATP hydrolysis in Eg5 kinesin involves a catalytic two-water mechanism. *J Biol Chem* 285(8):5859–5867.
19. Turner J, et al. (2001) Crystal structure of the mitotic spindle kinesin Eg5 reveals a novel conformation of the neck-linker. *J Biol Chem* 276(27):25496–25502.
20. Muretta JM, Petersen KJ, Thomas DD (2013) Direct real-time detection of the actin-activated power stroke within the myosin catalytic domain. *Proc Natl Acad Sci USA* 110(18):7211–7216.
21. Lakowicz JR (2006) *Principles of Fluorescence Spectroscopy* (Springer, New York).
22. Rice S, et al. (2003) Thermodynamic properties of the kinesin neck-region docking to the catalytic core. *Biophys J* 84(3):1844–1854.
23. Andreasson JOL, et al. (2015) Examining kinesin processivity within a general gating framework. *eLife*, 10.7554/eLife.07403.001.
24. Rosenfeld SS, Fordyce PM, Jefferson GM, King PH, Block SM (2003) Stepping and stretching. How kinesin uses internal strain to walk processively. *J Biol Chem* 278(20): 18550–18556.
25. Valentine MT, Fordyce PM, Krzysiak TC, Gilbert SP, Block SM (2006) Individual dimers of the mitotic kinesin motor Eg5 step processively and support substantial loads in vitro. *Nat Cell Biol* 8(5):470–476.
26. Muretta JM, et al. (2010) High-performance time-resolved fluorescence by direct waveform recording. *Rev Sci Instrum* 81(10):103101.
27. Nesmelov YE, et al. (2011) Structural kinetics of myosin by transient time-resolved FRET. *Proc Natl Acad Sci USA* 108(5):1891–1896.
28. Carter NJ, Cross RA (2005) Mechanics of the kinesin step. *Nature* 435(7040):308–312.
29. Rosenfeld SS, Xing J, Jefferson GM, Cheung HC, King PH (2002) Measuring kinesin's first step. *J Biol Chem* 277(39):36731–36739.
30. Kast D, Espinoza-Fonseca LM, Yi C, Thomas DD (2010) Phosphorylation-induced structural changes in smooth muscle myosin regulatory light chain. *Proc Natl Acad Sci USA* 107(18):8207–8212.
31. Johnson KA, Simpson ZB, Blom T (2009) Global kinetic explorer: A new computer program for dynamic simulation and fitting of kinetic data. *Anal Biochem* 387(1): 20–29.
32. Ma YZ, Taylor EW (1997) Kinetic mechanism of a monomeric kinesin construct. *J Biol Chem* 272(2):717–723.
33. Cochran JC, et al. (2004) Mechanistic analysis of the mitotic kinesin Eg5. *J Biol Chem* 279(37):38861–38870.
34. Sindelar CV, et al. (2002) Two conformations in the human kinesin power stroke defined by X-ray crystallography and EPR spectroscopy. *Nat Struct Biol* 9(11):844–848.
35. Muretta JM, et al. (2013) Loop L5 assumes three distinct orientations during the ATPase cycle of the mitotic kinesin Eg5: A transient and time-resolved fluorescence study. *J Biol Chem* 288(48):34839–34849.
36. Sindelar CV, Downing KH (2010) An atomic-level mechanism for activation of the kinesin molecular motors. *Proc Natl Acad Sci USA* 107(9):4111–4116.
37. Larson AG, Naber N, Cooke R, Pate E, Rice SE (2010) The conserved L5 loop establishes the pre-powerstroke conformation of the Kinesin-5 motor, eg5. *Biophys J* 98(11): 2619–2627.
38. Alonso MC, et al. (2007) An ATP gate controls tubulin binding by the tethered head of kinesin-1. *Science* 316(5821):120–123.
39. Krzysiak TC, Gilbert SP (2006) Dimeric Eg5 maintains processivity through alternating-site catalysis with rate-limiting ATP hydrolysis. *J Biol Chem* 281(51):39444–39454.
40. Hackney DD (2005) The tethered motor domain of a kinesin-microtubule complex catalyzes reversible synthesis of bound ATP. *Proc Natl Acad Sci USA* 102(51): 18338–18343.
41. Milic B, Andreasson JO, Hancock WO, Block SM (2014) Kinesin processivity is gated by phosphate release. *Proc Natl Acad Sci USA* 111(39):14136–14140.
42. Shastry S, Hancock WO (2011) Interhead tension determines processivity across diverse N-terminal kinesins. *Proc Natl Acad Sci USA* 108(39):16253–16258.
43. Krzysiak TC, Grabe M, Gilbert SP (2008) Getting in sync with dimeric Eg5. Initiation and regulation of the processive run. *J Biol Chem* 283(4):2078–2087.